THE ROYAL SOCIETY

Bubble dynamics, shock waves and sonoluminescence

By Claus-Dieter Ohl, Thomas Kurz, Reinhard Geisler, Olgert Lindau and Werner Lauterborn

Drittes Physikalisches Insitut, Universität Göttingen, Bürgerstraße 42-44, D-37073 Göttingen, Germany

Sound and light emission by bubbles is studied experimentally. Single bubbles kept in a bubble trap and single laser-generated bubbles are investigated using ultrafast and high-speed photography in combination with hydrophones. The optical observation at 20 million frames per second of the shock waves emitted has proven instrumental in revealing the dynamic process upon bubble collapse. When jet formation is initiated by a non-spherically symmetric environment, several distinct shock waves are emitted within a few hundred nanoseconds, originating from different sites of the bubble. The counterjet phenomenon is interpreted in this context as a secondary cavitation event. Furthermore, the light emission of laser-generated cavities—termed cavitation bubble luminescence—is studied with respect to the symmetry of collapse. The prospects of optical cavitation and multibubble trapping in the study of few-bubble systems and bubble interactions are briefly discussed. Finally, the behaviour of bubble clouds, their oscillations, acoustic noise and light emission are described. Depending on the strength of the driving sound field, period doubling and chaotic oscillations of the collective bubble dynamics are observed.

Keywords: sonoluminescence, single-bubble; cavitation, laser-induced; shock wave; high-speed photography; intensified photography

1. Introduction

Bubbles in a liquid, their movement and oscillations are easily amenable to our imagination. Nevertheless, as two-phase systems with free boundaries, they constitute a subject notoriously difficult to study scientifically due to their involved dynamics on largely different very short time-scales.

In practical applications as well as laboratory experiments, multibubble systems prevail. In fact, they have been the focus of cavitation research for many decades, with a considerable body of knowledge being accumulated over this time. In multibubble cavitation the influence of the environment, i.e. the interaction of bubbles with the applied sound field, with obstacles or boundaries, and the mutual interaction of bubbles, renders a very complicated situation full of interesting physics: in particular, sound and light emission; free-boundary flow with, e.g. surface oscillations or high-speed liquid jets; shock waves; chemical reactions and structure formation in the bubble field (Brennen 1995; Leighton 1994).

Before one can hope to achieve a better understanding of complex systems composed of elementary units, it is necessary to study these units in detail. This scientific rationale has proven successful in a number of circumstances. For cavitation it means

that we have to look thoroughly at the single isolated bubble and its interaction with the environment in a controlled setting. One way of doing so is by means of bubble traps. They have become popular recently through the discovery of the remarkable phenomenon of single-bubble sonoluminescence (SBSL) (Gaitan *et al*. 1992), which gave new thrust to cavitation physics and, in particular, to the exploration of sonoluminescence. A second complementary method of single-bubble investigation is provided by optic cavitation, i.e. the generation of transient cavities in liquids by strong laser pulses (see Lauterborn 1980). Bubble luminescence is also observed in optic cavitation (Buzukov & Teslenko 1971) and thus it is expected that light-produced bubbles will become increasingly popular for the investigation of this phenomenon as they extend the range of available bubble sizes.

The first part of this paper gives an overview of results on single-bubble dynamics obtained by the two methods to discuss the prospects they hold for further exploration, especially of cavitation bubble luminescence. Both approaches will be extended to the systematic study of few-bubble systems with their mutual interaction, naturally opening the way for the investigation of more complicated bubble arrangements.

In the second part of the paper, we review some modern results on multibubble acoustic cavitation and thus come full circle with the historic development of the subject. We believe that, backed up by a better understanding of single- and few-bubble systems, by application of state-of-the-art experimental equipment (e.g. sensitive high-speed gatable cameras or ultrashort pulsed lasers) and by refinement of theoretical models together with their extensive numerical investigation, significant progress in this area is possible.

2. Spherical bubble dynamics

Optic cavitation and single-bubble acoustic levitation offer methods for studying the 'elementary unit' of cavitation, the single bubble. In particular, in both cases, spherically symmetric (or radial) bubble dynamics can be realized at least approximately, apart from possible deviations from sphericity during bubble collapse due to inherent instabilities. To describe radial bubble dynamics, theoretical models of different degrees of complexity have been devised, originating from Lord Rayleigh's (1917) treatment of the collapse of an empty cavity. Thus, both methods of investigation enable us to assess the various models of radial bubble motion and to clarify which physical processes are important and which ones can be neglected under given experimental conditions.

(*a*) *Laser-generated bubbles*

Optic cavitation provides a convenient means of generating a single bubble in a transparent liquid (Lauterborn 1980). For that purpose, a short laser pulse is focused into the liquid. Figure 1 depicts an experimental arrangement for observing the bubble and its shock waves by high-speed photography. The shock waves are also monitored by a fast hydrophone.

Almost any laser which can emit short pulses with durations of the order of a few nanoseconds or less, and energies per pulse of a few millijoules, can be used. The light pulses must be tightly focused by aberration-minimized lenses to avoid multiple

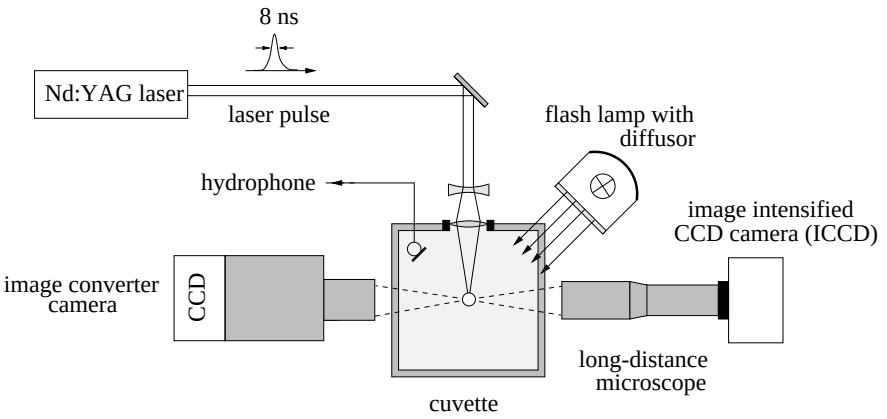

Figure 1. Typical experimental arrangement for optic cavitation with high-speed photography of bubble dynamics. For the photography of shock waves, the diffuser is removed and a small aperture of the camera objective is chosen.

Figure 2. Bubble generation and shock wave emission upon laser-induced breakdown caused by a focused Nd:YAG laser pulse in water. The CCD photographs of the breakdown were taken with 100 fs pulses for back-illumination, obtained via a pulse picker from a Ti:sapphire laser. The frame size is $0.66 \times 0.66\ \mathrm{mm}^2$. From left to right, the following time delays between the generating pulse and the illumination pulse apply (measured from peak to peak): 9.5 ns, 13 ns, 69 ns, 107 ns and 157 ns. The bright light emission is due to the laser-produced plasma. The forming bubble is visible as a dark border around the central spot. In the short time interval covered the bubble does not grow significantly.

and spatially extended breakdown sites. A planoconvex lens inserted in the wall of the cuvette could serve that purpose as a good first approximation. In the focal region, a very-high light intensity, associated with a large strength in the electric field, is achieved. There the laser pulse causes heating of impurities and/or dielectric breakdown with avalanche ionization, and creates a plasma spot. The plasma expands to form the cavity. Figure 2 gives an example of bubble generation by a Nd:YAG laser pulse and the associated shock-wave emission. To stop the rapid expansion of the cavity and the shock propagation, the photographs were taken with single laser pulses of about 100 fs duration.

Bubble dynamics is exceedingly fast, and the collapse of a bubble can be captured only with high-speed cameras or short illumination. Figure 3 gives an example of a high-speed photographic sequence which probes the final collapse stages. This series was taken at 20.8 million frames per second with an image converter camera (Ohl *et al*. 1995). The maximum number of frames per shot is limited to eight. Therefore, four different shots corresponding to nearly identical bubbles have been combined

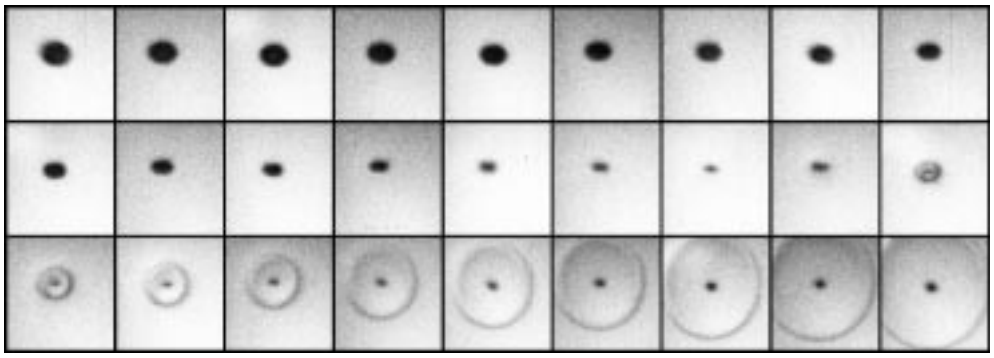

Figure 3. A spherically symmetric shock wave emitted by a laser-generated bubble upon first collapse taken at 20.8 million frames per second with the arrangement depicted in figure 1. The frame size is $1.5 \times 1.8\ \mathrm{mm}^2$ and the exposure time is *ca.* 5 ns.

into one series. This approach is justified by the excellent reproducibility of the bubble size.

In figure 3, a free spherical bubble produced in water is shown to undergo a rapid first collapse and, in this process, radiate a spherically symmetric shock wave. The series starts after the bubble has reached maximum radius. The bubble is seen as a dark disc because the illuminating backlight is deflected off the bubble wall. From the point of maximum expansion, the bubble starts to shrink, gaining speed at an ever increasing rate, driven by the ambient pressure and leading to a collapse with strong compression of the bubble contents (gas and vapour) in the final phase. The pressure within the bubble rises steeply, with the gas content acting as a hard spring, abruptly stopping the inward motion and driving the bubble back into expansion, called rebound.

As is clearly visible from figure 3, in the stage of maximum compression an outward going shock wave is emitted. The shock wave propagates at about the velocity of sound, i.e. at about $1500\ \mathrm{m\,s^{-1}}$ in water. To capture it, including its propagation, one needs short exposure times and very-high-speed framing. A framing rate of 20 million frames per second proved necessary to partly resolve details of the rapid dynamics. Then a shock wave can be seen on several frames, and multiple shock waves, as encountered in asymmetric collapse, can be assigned to their emission sites.

(*b*) *Acoustically driven bubbles*

Laser-generated bubbles are transient in nature, and the initial energy deposited into the bubble by the light is dissipated away within a few oscillation cycles. Therefore, laser-generated bubbles are not in equilibrium with the surrounding liquid. Their gas and vapour content is mainly determined by the physical processes immediately at, or shortly after, laser breakdown. Unfortunately, no direct measurements of bubble composition at this instant are presently possible.

Acoustically driven levitated single bubbles have quite different properties. Relatively small bubbles with an equilibrium radius of only a few micrometres can be trapped in the pressure antinode of a standing wave field, pushed there by primary Bjerknes forces. They can settle into stable radial oscillations at a more or less fixed

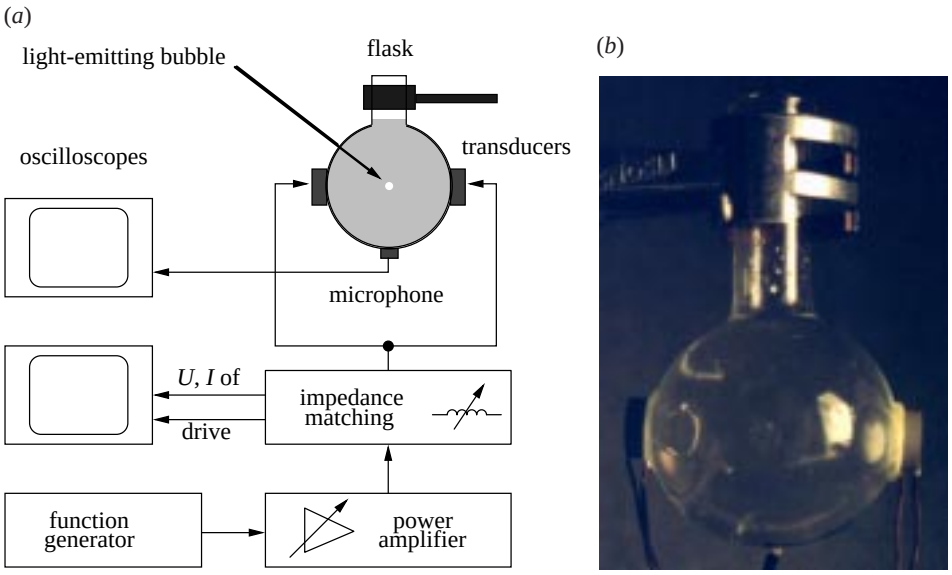

Figure 4. (*a*) Experimental arrangement for the investigation of SBSL. (*b*) Photograph of spherical flask with light-emitting bubble.

position if the physical parameters (ambient pressure, dissolved gas content of the liquid, driving pressure) are chosen appropriately. The bubble is then in a stable dynamic equilibrium; its bias to grow by rectified diffusion is balanced by the tendency to dissolve because of surface tension, in combination with the appropriate response to give a stable mean radius.

Figure 4 shows an arrangement for stable bubble levitation which has become widely used in the investigation of SBSL. Instead of the spherical flask, cylindrical or rectangular containers can also be used; we also succeeded in producing SBSL in ovoids. The flask is driven by piezoceramic transducers glued to its sides. A small transducer pill is used as a microphone to detect the acoustic emission of the bubble. By inspection of the acoustic signal alone it is possible to tell whether a bubble is stably trapped. Its presence reveals itself by small ripples or spikes in the microphone signal due to the acoustic emission of the bubble, which is driven far below its linear resonance frequency.

For stable trapping it is essential to control the dissolved gas content of the liquid. Therefore, a closed flask is preferable over an open flask, with control over the ambient pressure. Furthermore, the driving frequency and driving amplitude have to be adjusted carefully. For non-optimal parameters, especially a too high gas content, the bubble's position is unstable and a dancing motion will be observed.

The discovery of bright single-bubble luminescence has spurred much research activity, both theoretical and experimental, to uncover the hydrodynamical aspects of the phenomenon and the properties of the emitted light. In experiments, SBSL bubbles were investigated with hydrophones, photomultipliers, Mie scattering of continuous wave or pulsed laser light, or with streak cameras. SBSL pulses have been found to have remarkable properties, straining current experimental techniques to their limit. First of all, the SBSL flashes are of very short duration, in the range of 60–250 ps (Gompf *et al*. 1997). Recent experiments have found evidence for slightly

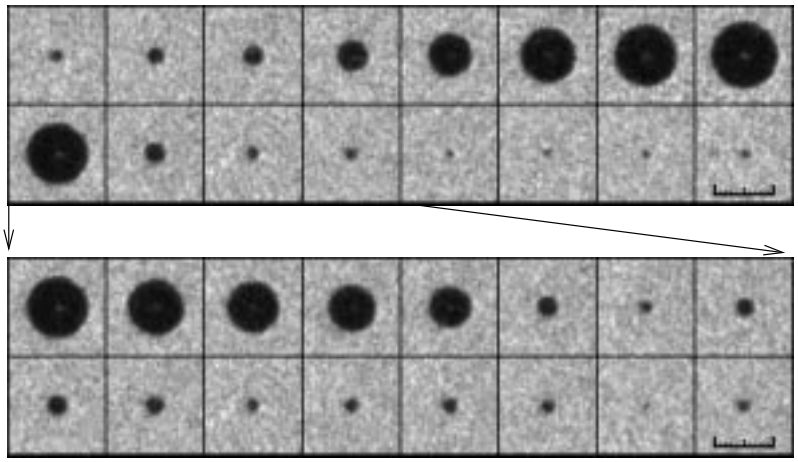

Figure 5. Photographic series of a trapped sonoluminescing bubble driven at 21.4 kHz. The top row presents the bubble dynamics at an interframe time of *ca.* 2.5 μs. The bottom row shows the bubble collapse with five-fold temporal resolution (500 ns interframe time). The scale of the image is indicated by the ruler (100 μm).

different pulse durations at different wavelengths for low temperature of the liquid (Moran & Sweider 1998). Each SBSL pulse consists of *ca.* 10^5–10^6 photons, the intensity being strongly dependent on temperature, the type of dissolved gas and its concentration (Barber *et al.* 1994). The pulse spectrum extends well into the UV region and is compatible with a black-body or bremsstrahlung spectrum, indicating temperatures in excess of 10 000 K (Hiller *et al.* 1992). The radial dynamics of sonoluminescing bubbles were investigated by laser-light scattering (see, for example, Weninger *et al.* 1997) and photography (Tian *et al.* 1996); bubble stability was assessed by means of phase diagrams in parameter planes spanned by acoustic pressure and equilibrium radius (Holt & Gaitan 1996).

In brief, a large amount of experimental data about SBSL have been gathered over recent years (Barber *et al.* 1997). On the theoretical side, a corresponding amount of modelling and speculation took place. There are quite a number of competing theories that, for example, invoke different collapse modes or give different causes for the light emission, etc. One of the most widely accepted models assumes the generation of a converging shock wave upon bubble collapse (Heim 1961), giving rise to a hot spot and the generation of a partly ionized plasma in the bubble centre (Wu & Roberts 1994; Moss *et al.* 1997). This would imply a certain degree of sphericity of the collapse as a necessary prerequisite for SBSL emission.

One approach to investigating the question of sphericity experimentally, that up until now has not been exploited sufficiently, is the direct optical observation of the surface dynamics and, in particular, the collapse of a trapped sonoluminescing bubble at high spatial and temporal resolution. As an example, figure 5 shows the radial oscillation of a trapped bubble obtained by photography with a gated CCD camera and flash illumination. The gating time was set to 5 ns, the smallest possible for the device used. Of course, this sequence was not acquired within one oscillation cycle, but a stably oscillating bubble was illuminated stroboscopically and the time delay between driving signal and flash light trigger was incremented before each exposure.

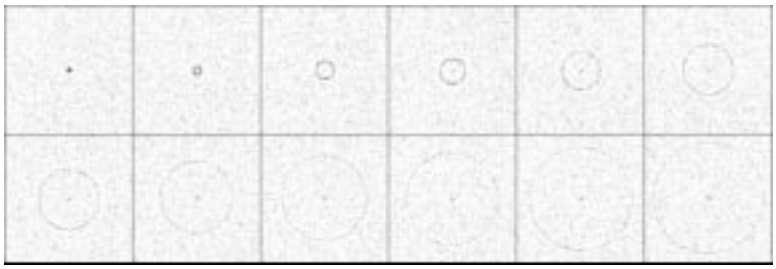

Figure 6. Spherical shock wave emitted by a sonoluminescing bubble into the surrounding liquid. The temporal separation of adjacent frames is *ca.* 30 ns; the frame size corresponds to an area of $1.6 \times 1.6\ \mathrm{mm}^2$ in the object plane.

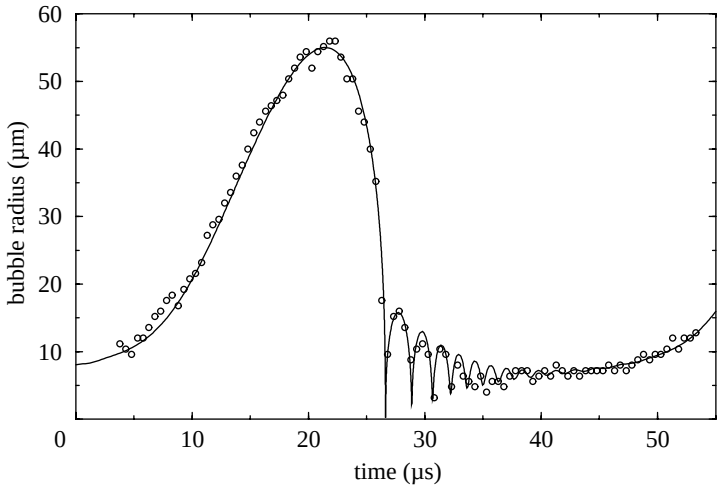

Figure 7. Radius–time curve of a trapped bubble in a water–glycerine mixture derived from photographic observations. A numerically calculated curve is superimposed on the experimental data points (open circles). The calculation is based on the following parameters: driving frequency, $f_0 = 21.4$ kHz; ambient pressure, $p_0 = 1$ bar; driving pressure, $p_\mathrm{a} = 1.32$ bar; vapour pressure, $p_\mathrm{v} = 25$ mbar; equilibrium radius, $R_0 = 8$ µm; density of the liquid, $\rho = 1000\ \mathrm{kg\ m^{-3}}$; viscosity, $\eta = 0.006\ \mathrm{Ns\ m^{-2}}$; surface tension, $\sigma = 0.07\ \mathrm{N\ m^{-1}}$. The gas within the bubble is assumed to obey the adiabatic equation of state for an ideal gas with a ratio of the specific heats of 1.33.

The same experimental arrangement, with proper parallel back-illumination of the bubble, was used to obtain a photographic series of the shock wave emission of the SBSL bubble (figure 6). It gives no indication of any deviation from spherical symmetry.

In figure 7, the dependence of bubble radius on time, derived from the experiment, is compared to a numerical calculation based on a Rayleigh–Plesset equation (see, for example, Leighton 1994), with parameters R_0 (equilibrium radius), p_a (acoustic drive amplitude) and η (viscosity) chosen for best fit. Within the error bounds of the measurement, the data set coincides quite well with the numerical curve. Figure 6 illustrates the characteristic dependence of radius on time for a trapped SBSL bubble with its many fast afterbounces after the main collapse, where the bubble would 'prefer' to oscillate at its own resonant frequency.

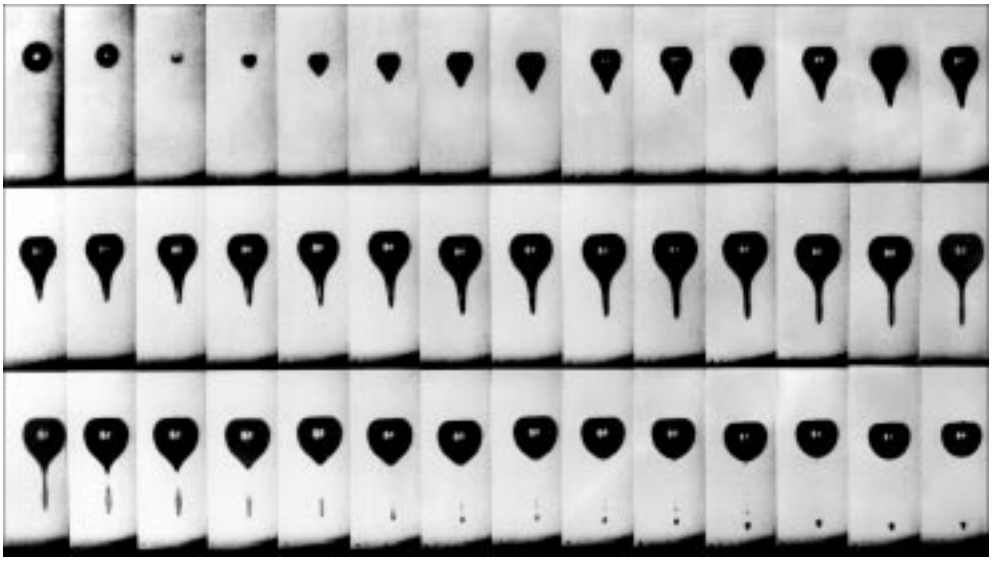

Figure 8. Dynamics of a laser-generated spherical bubble in water of reduced surface tension in the vicinity of a plane solid boundary (at the bottom), observed at 300 000 frames per second. The size of each frame is $6.7 \times 2.7\ \mathrm{mm}^2$.

Until now we have only considered light emission by stably oscillating trapped bubbles which presumably have a high degree of spherical symmetry. Light emission by spherical laser-generated bubbles is also observed. It will be discussed in the next section in the general context of single-cavitation bubble luminescence.

3. Aspherical bubble dynamics

When a bubble is collapsing in a non-spherically symmetric environment the collapse changes in a remarkable way. A flat solid surface in the vicinity of (say, below) the bubble causes it to involute from the top and to develop a high-speed liquid jet towards the surface. When the jet hits the opposite bubble wall from the inside it pushes the bubble wall ahead, causing a funnel-shaped protrusion with the jet inside. Figure 8 shows a high-speed photographic series of a bubble collapsing in water of reduced surface tension near a flat solid wall, taken at 300 000 frames per second with a rotating mirror camera. The jet is best visible in the first rebound phase as the dark line inside the bright central spot of the bubble, where the backlight can pass undisturbed through its smooth surface. The funnel-shaped protrusion directed downwards is the elongated bubble wall containing the jet that drives the elongation until its energy is used up. Then the long tube of gas and vapour becomes unstable and decays into many tiny bubbles, while the main bubble surface snaps back to its former spherical shape. Figure 9*a* is an enlargement of the bubble with the jet and the protrusion pointing towards the solid boundary.

The normalized distance $\gamma = s/R_{\max}$, where s is the distance of the laser focus from the boundary and $R_{\max}$ is the maximum bubble radius attained (figure 9*b*), is the main parameter for classifying the bubble dynamics near a plane rigid boundary. Bubbles with different $R_{\max}$ but the same γ value exhibit similar dynamics, thus giving the chance to specify the degree of asymmetry of bubble collapse: cavitation

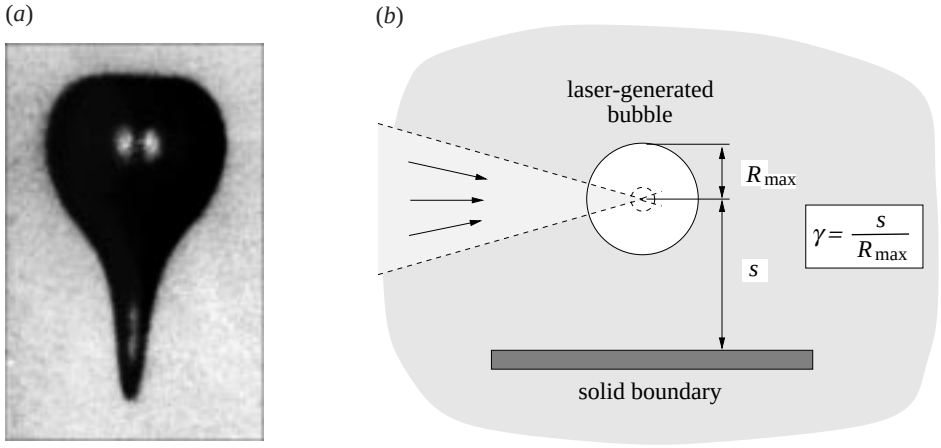

Figure 9. (*a*) Laser-generated bubble collapsing asymmetrically in the vicinity of a solid boundary (at the bottom). During collapse a jet forms, penetrating the bubble in the direction of the boundary. (*b*) Geometrical relations for the definition of the parameter γ.

bubbles with a small value of γ are more influenced by the boundary, collapsing with a more pronounced shape variation, than those with a large value, which collapse in a more sphere-like fashion. This statement, however, does not apply to bubbles too close to the boundary, where $\gamma \approx 0$ and the bubble adopts a hemispherical shape, i.e. again approaches a spherical symmetry.

Note that in the given definition of γ, and also in the following discussion of laser-generated bubbles, the laser light is assumed to be incident parallel to the solid boundary. Otherwise, the distance s could not be defined so well, since the laser focus in general has an elongated approximately conical shape with larger longitudinal than transverse extension. All results stated below are valid under this proviso; whether they hold under more general conditions is still under active investigation.

(*a*) *Shock-wave scenario at collapse*

Bubble collapse is a concept which is not easy to define. The moment of bubble collapse in the spherical case can be ascribed to the instant when the bubble reaches its minimum radius. This definition, however, does not apply to the aspherical case, where the bubble morphology changes and a unique radius of the bubble cannot be given. Therefore, in the aspherical case we assign the bubble collapse to the very late stage of compression of the bubble interior. High-speed photography has revealed different dynamical features of this motion. At first, the bubble loses spherical symmetry: an indentation and subsequently a liquid jet is formed. The jet traverses the bubble, hits the opposite wall and pushes it ahead. In this way a vortex ring is generated and the bubble acquires a toroidal shape. In the further course of collapse the bubble torus becomes unstable, whereby several distinct shock waves are emitted into the liquid. Simultaneously, a new structure may appear—the 'counterjet'. Moreover, the asymmetric bubble collapse may also be accompanied by light emission.

With the loss of spherical symmetry, the bubble eventually becomes concave, and thus with decreasing volume the bubble boundaries will finally impact onto each other if the reaction of the bubble interior does not drive the bubble into expansion before

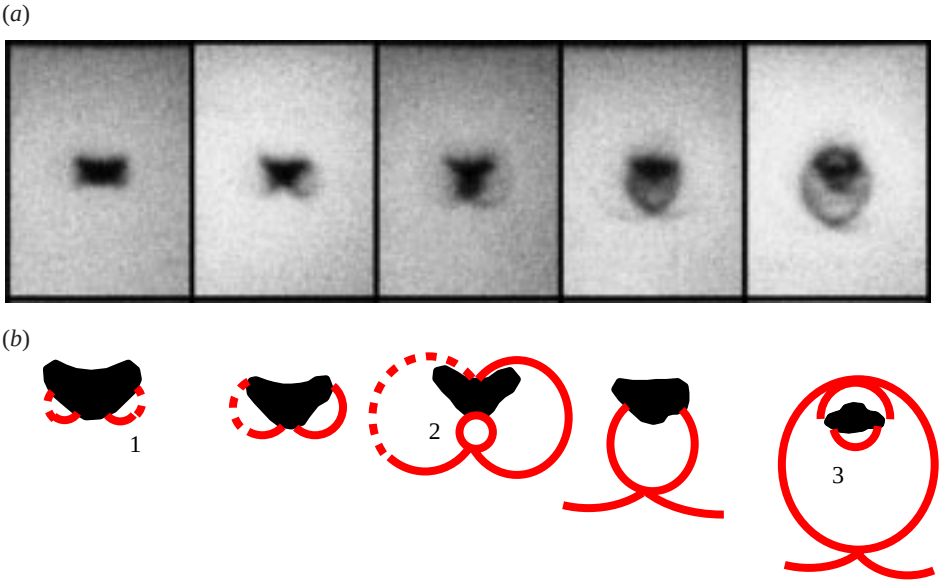

Figure 10. Scenario of asymmetric bubble collapse with indication of the different shock waves emitted. The size of the individual frames is $2.0 \times 1.4\ \mathrm{mm}^2$ and the asymmetry parameter is $\gamma = 2.7$.

this occurs. Therefore, the aspherical collapse allows us to study the interaction of phase boundaries impacting at high velocity (Rein 1993). Figure 10*a* exhibits this distinct event, showing five consecutive images taken at an interframe time of 48 ns. A pictorial presentation of the photographic series is given in figure 10*b*, where an enlarged outline of the bubble shape and the emitted shock waves are plotted separately. In the first time-frame the first shock wave emission, called the *jet shock wave*, is already apparent. It is caused by the jet impact onto the lower bubble wall. Closing the wings of the jet shock wave to circles determines the centre of the shock-wave emission. We propose that the broad tip of the jet forms a circular line of impact onto the lower bubble wall, which is the origin of a toroidal shock wave. Viewed sideways it appears in the form of two wings.

A second shock wave, the *tip bubble shock wave*, becomes visible below the bubble in the third frame. Because of the jet impact onto the lower bubble wall, the morphology of the bubble has changed to toroidal, with a gas pocket enclosed by the broad jet tip and the lower bubble wall. The compression of this gas pocket leads to the emission of the second shock wave. The bubble has still not reached its minimum volume; the bubble content is compressed even further. This final compression is accompanied by the emission of a third shock wave, the *compression shock wave*, visible in the last frame of figure 10. However, as the compression of a toroidal bubble is strongly unstable (Philipp & Lauterborn 1998), one expects the emission of multiple shock waves from different locations along the torus. This last compression stage is located in a small volume only, thus the several shock waves presumably present close up and are visible as two shock fronts, the first in the direction of the jet flow and the second on top of the bubble.

A photographic series at a γ value of 2.4 is reproduced in figure 11. This smaller γ

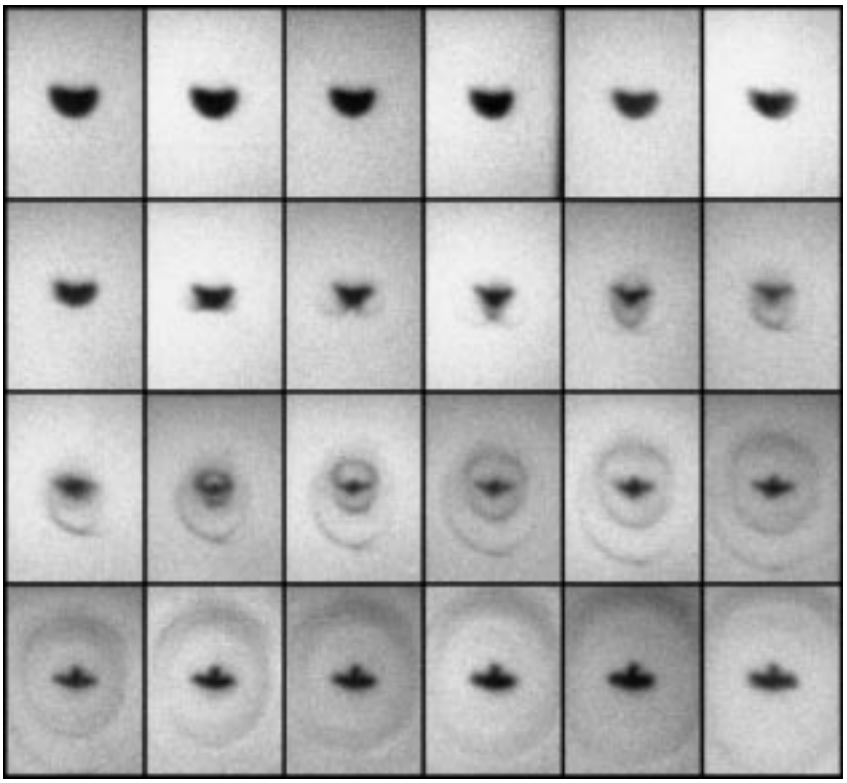

Figure 11. Collapse of a laser-generated cavitation bubble near a solid boundary (out of view below each frame) taken at 20.8 million frames per second. Relative distance to the boundary is $\gamma = 2.4$. Three shock waves are emitted: the jet torus shock wave (frames 8–10), the tip bubble shock wave (frame 10 onwards) and the main bubble shock wave (frame 13 onwards). The frames are counted from left to right and from top to bottom. The frame size is 2.0×1.4 mm.

value (cf. figure 10) leads to a more asymmetric bubble collapse. The emission of the three types of shock waves discussed above is clearly visible here because the events causing them are more separated in time.

(*b*) *Counterjet*

The protrusion visible on top of the bubble from frame 15 onwards in figure 11 was given the name counterjet since, at a first glance, it has the same appearance as the jet towards the solid boundary but in the opposite direction. However, the high-speed photographic series of figure 11 reveals a marked difference between the counterjet and jet formation (cf. figure 8). The protrusion of the lower bubble wall is formed continuously during the first half of the second oscillation cycle, while the counterjet is visible immediately after the emission of shock waves at the bubble minimum, and, in contrast to the smoothly developing jet protrusion, the counterjet does not change its shape or its position.

The discussion of events leading to the emission of multiple shock waves in the previous section guides the following model of counterjet formation: a *jet shock wave* propagates through the jet funnel, which can be considered as a wave guide, reflect-

ing the wave at the liquid–gas interface. Therefore, regions of strong tension can build up inside, and at the head of, the funnel. Cavitation nuclei present in the liquid expand under this tensile stress and gain a sufficiently large radius to become visible.

We introduce a simple model to calculate the counterjet formation: it is assumed that a pressure pulse with an amplitude related to the water hammer pressure is radiated from the lower bubble wall into the jet funnel. The duration of the pressure pulse is approximated by the time needed for an expansion wave to travel half the diameter of the jet tip. The pressure distribution inside the jet funnel is calculated by solving the linear wave equation in cylindrical coordinates with finite differences on a static grid, where the shape of the jet is extracted from high-speed photographs, approximated with simple geometric functions and included as an ideal free boundary into the algorithm.

The pressure distribution for a number of instants is plotted in the top part of figure 12. Graph (a) depicts the geometry of the boundary condition forming a cone-like jet funnel with the jet flowing from the right to the left. Small values on the grid represent the liquid and large values the gas phase. In the following graphs (b)–(f) the spatial pressure distribution is plotted at successive time-steps. The major point is clearly visible: the initial high-pressure peak (water hammer pressure) is transformed into an expansion wave with a trailing region of tensile strain. The strain amplitude becomes as large as 300 bar.

The response of cavitation nuclei, i.e. trapped gas pockets in crevices of impurities, to a time-varying pressure depends on their enclosed volume. Large cavitation nuclei will not be expanded significantly, as their natural frequency does not match the forcing pressure pulse. On the other hand, small nuclei will be expanded to nearly the same maximum size, because, when the surface tension of the nuclei is overcome by the driving tension, the expansion of the nuclei becomes dominated by inertia. The bottom part of figure 12 presents the numerically calculated counterjet superimposed on an image of a bubble 1 μs after the jet impact. The cavitation nuclei are assumed to be equally distributed in space, and only nuclei which have acquired a radius larger than 1 μm are plotted. The agreement between the simple model and the experiment is reasonable.

As a result, a bubble collapsing with a jet funnel can cause further cavitation on a smaller spatial scale. Thus, the counterjet is explained in terms of *secondary cavitation* as an analogue to the foam observed beneath the water surface when a shock wave, caused, for example, by an underwater detonation, is reflected into a tension wave, expanding cavitation nuclei (Kedrinskii 1997). This idea allows us to derive prerequisites for counterjet formation and to compare calculations with experimental results. With decreasing size of the jet funnel, at increasing values of γ, the counterjet becomes less pronounced because the area of the free boundary which is responsible for the transformation of the high pressure into tension becomes smaller. In the limit of a completely spherical collapse ($\gamma \to \infty$) no counterjet will be formed. On the other hand, for larger γ values the jet reaches higher velocities leading to a higher amplitude of the pressure pulse emitted after the liquid–liquid impact. These two opposite effects will manifest themselves by a maximum of counterjet visibility upon variation of γ. This maximum visibility has been reported by Vogel *et al*. (1989) for $1.2 \leqslant \gamma \leqslant 1.7$, being less pronounced above and below the given range.

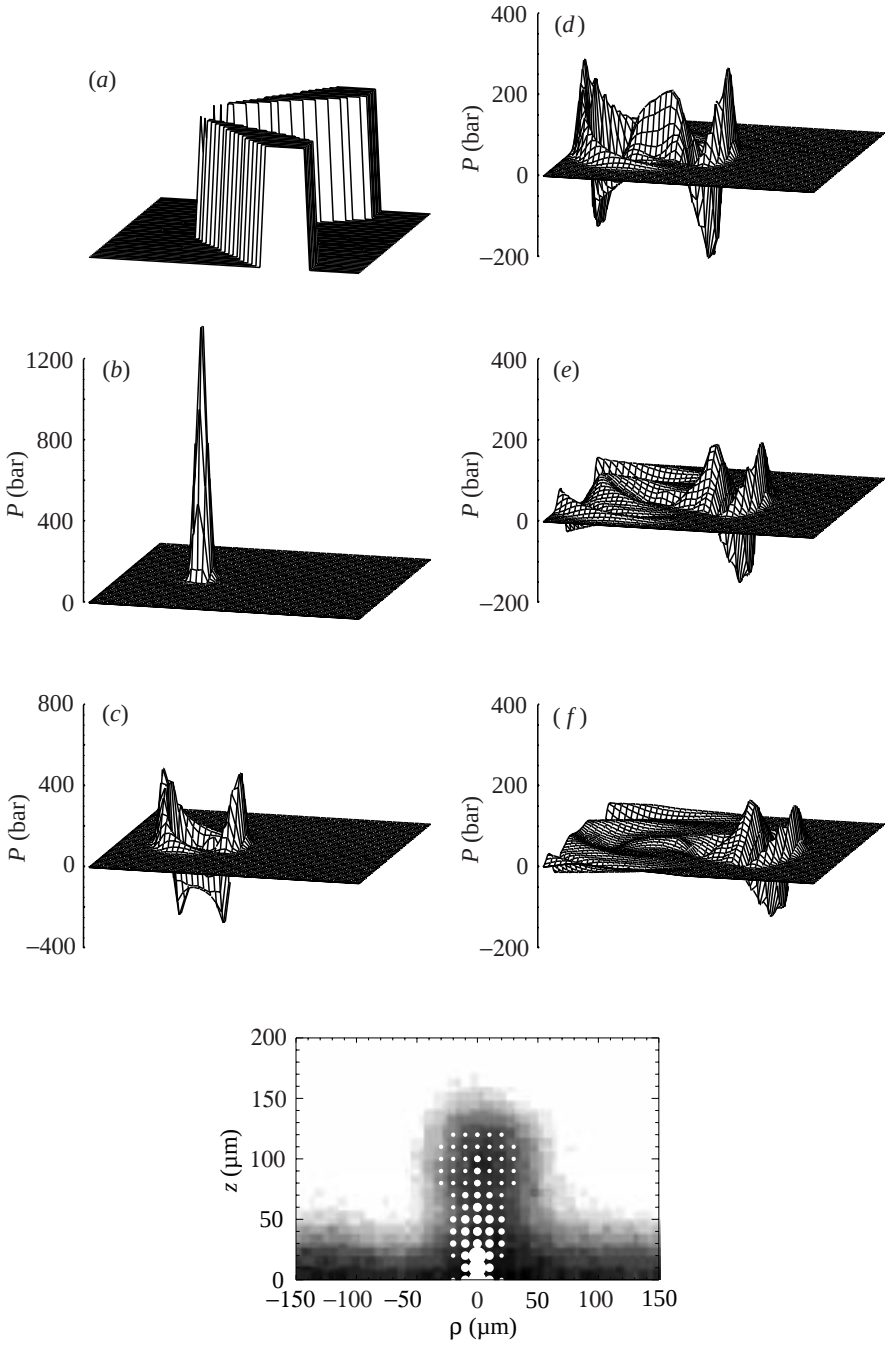

Figure 12. (Top) Pressure distribution in the jet funnel for different time-steps and $\gamma = 2.5$. The region shown is 0.5×0.5 mm^2 wide. (*a*) The jet funnel is plotted with the liquid phase as low values and the gas phase as high values. Pressure distribution after jet impact at: (*b*) 12 ns; (*c*) 40 ns; (*d*) 60 ns; (*e*) 80 ns; (*f*) 100 ns. (Bottom) Image of a cavitation bubble with $\gamma = 2.5$, 1 μs after the impact and superimposed calculated counterjet (white dots).

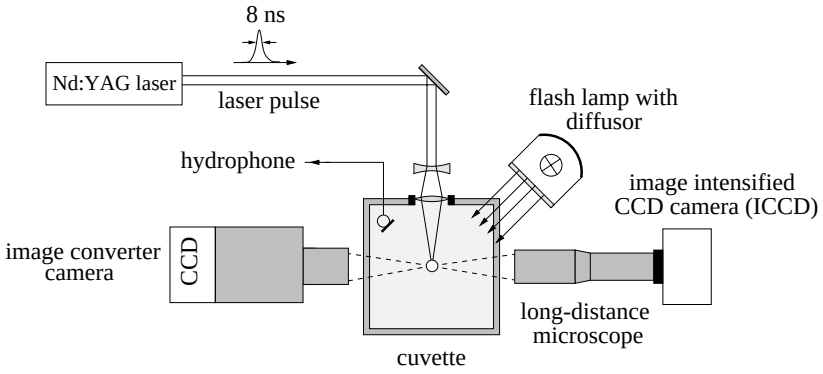

Figure 13. Extended experimental arrangement for cavitation bubble luminescence studies.

The proposed model explains the nearly instantaneous appearance of the counterjet during the collapse, its antipodal direction and the limited region of γ values where it is observed experimentally. A further experimental test for this model would be to check for decreased secondary cavitation in very pure liquids with considerably less gaseous nuclei below 1 μm.

(*c*) *Light emission*

A major question in the discussion of the origin of SBSL is the sphericity of the bubble upon collapse. One widely accepted model for light emission is the concentration of energy by inwardly converging shocks, focusing at the geometrical centre of the bubble. With laser bubbles near boundaries, this question can be attacked through systematic investigation of the light-emission dependence on the asymmetry parameter γ. We have not only found light emission from spherically collapsing bubbles, but also from bubbles with weak asphericity before collapse (Ohl *et al*. 1998). Since the light emission was not caused by acoustic excitation, but by the energy input of the generating laser pulse, we propose to call this phenomenon single-cavitation bubble luminescence (SCBL).

For photography of the luminescence event we equipped the experiment with a long-distance microscope and an ICCD (intensified CCD) camera (figure 13). This camera had a high contrast ratio between the shuttered and the opened state, which is a favourable property for suppressing the intense continuum light emission from the dielectric breakdown process. An optical resolution of the luminescence image better than 3 μm was achieved. Figure 14 shows an image of the luminescence which occurs during the spherical-bubble collapse taken with the ICCD camera. The gate open time was adjusted to 5 μs and an attenuated flash illuminated the bubble. The bright SCBL spot in figure 14*a* is in the centre of the bubble outline. Light emission is observed when the gating time of the ICCD covers the bubble collapse, monitored with a hydrophone.

By measuring the spot size, integrating the collected light over the spot area and, in the same run, determining the maximum radius, we obtained the graph shown in figure 14*b*. It gives the dependence of the radius of the light-emitting region within the bubble, and the number of photons emitted, on the maximum bubble radius $R_{\max}$ attained. The figure demonstrates clearly that the size of the bubble at maximum

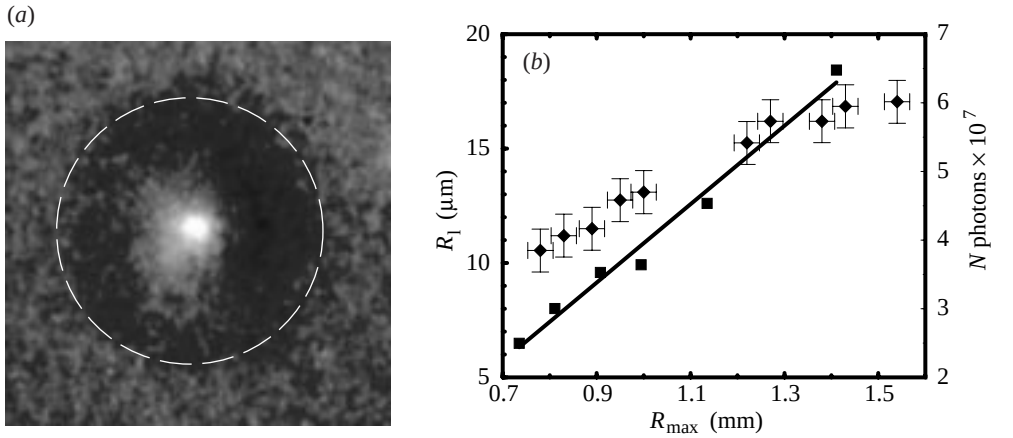

Figure 14. SCBL. (*a*) Light emission from a laser-generated bubble upon first collapse. Superimposed on the image is an outline of the maximum bubble size before collapse. (*b*) Radius R_l of the emission spot (diamonds) and number N of photons emitted (squares) as a function of the maximum radius of the bubble.

expansion is strongly correlated with the light output, the dependence being linear to a good approximation. Obviously, the larger the bubble radius R_{max} the more violent is the collapse, and the more light is emitted illuminating a larger volume.

We now turn to the luminescence of asymmetrically collapsing cavities. By proper placing of the laser focus we are able to control γ and thus the degree of asphericity. Figure 15 reports the result of the corresponding experiment on light emission. The picture series in figure 15*a* was obtained by a combination of two photographic devices, namely an image-converter camera and a separate ICCD as shown in figure 13. Frames 1–7 show the bubble dynamics for $\gamma = 4.7$ photographed with the image-converter camera at 220 000 frames per second. Before collapse (frames 1–4), the bubble has a spherical shape. In frame 5a the image taken with the high-speed camera was blended over a photograph of the luminescence spot, obtained with the ICCD (same experimental parameters but from a different run). After the collapse the liquid jet again forms a protrusion towards the solid boundary (frames 6, 7), which is out of view below the frames.

During bubble collapse the bubble centre translates towards the boundary. Thus, the light emission is located 135 μm below the centre of the bubble prior to collapse, and the position of the light emission is at the geometrical centre of the main body of the re-expanding bubble. The sequence does not resolve the shape of the bubble at the instant of light emission, as even a framing rate of 20 million frames per second is too slow to capture the details of multiple shock-wave emission for γ values larger than about three. Indirect evidence for an almost spherical collapse is the missing counterjet (see the previous section) above the re-expanding bubble. In our current research project we set out to resolve the final collapse stages by photography with ultrashort laser pulses. An example of the method is given in figure 2.

Figure 15*b* gives the normalized (with respect to the spherical case) radiated energy for a fixed R_{max} as a function of normalized distance γ. For $\gamma \leqslant 3.5$ the light output is not distinguishable from the dark signal to the best sensitivity of our equipment. The

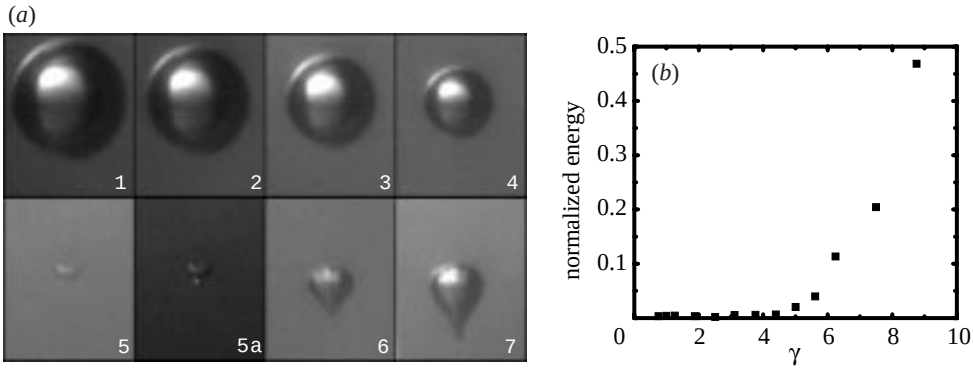

Figure 15. Luminescence of an asymmetrically collapsing laser-generated bubble. (*a*) Photographic sequence indicating the maximum bubble size and the location of the light-emitting spot with $\gamma = 4.7$. Frame 5a is a copy of frame 5 with an image of the light-emitting spot superimposed. (*b*) Dependence of light intensity, normalized to the emission at spherical collapse, on the distance parameter γ.

integrated luminescence decreases rapidly with smaller γ values. It is not detectable for too strong an asphericity of bubble collapse.

We found that for an aspherical bubble collapse, shock-wave emission is not necessarily connected with a luminescence event. There is only a certain regime of asphericity where luminescence occurs. Here, an opportunity to gain more insight into the processes inside the bubble arises from the study of aspherial collapse with state-of-the-art three-dimensional-numerical algorithms. Comparing these results with the bubble outline obtained from experiments could determine the conditions for light emission and finally give evidence for the mechanisms which are responsible for cavitation bubble luminescence.

4. Few-bubble systems

Oscillating bubbles in an acoustic field are not only attracted towards the pressure node or antinode, depending on their size, but they exert forces upon each other which can be attractive or repulsive. These secondary Bjerknes forces are usually described by a linearized theory, with the bubbles undergoing small linear oscillations. Little is known experimentally about bubble interactions and bubble dynamics in the case of strongly nonlinear oscillations (Mettin *et al*. 1997) or of close proximity where the interacting cavities can influence the collapse behaviour of each other. Furthermore, the interaction of oscillating bubbles with shock waves emitted by other nearby bubbles still has to be investigated in experiments involving only a small number of bubbles.

For this purpose, both methods discussed in the case of single-bubble dynamics can be extended or even combined to study few-bubble systems, beginning with two bubbles separated by a certain distance. For example, it is possible to confine two or more bubbles in different pressure antinodes of a large-aspect-ratio cuvette (see figure 16). This arrangement is most suitable for the investigation of the effect of a shock wave emitted by one bubble on the dynamics of a second bubble.

In order to study the interactions of closely spaced bubbles, optic cavitation is the method of choice. With suitable focusing of short laser pulses (e.g. by holographic–

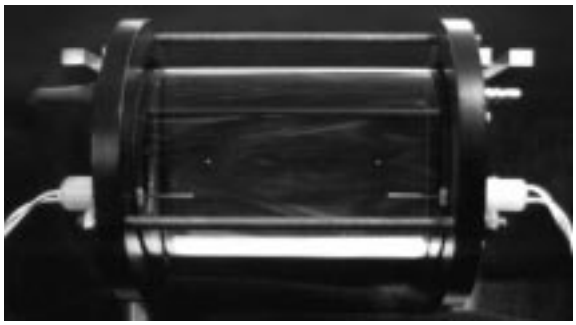

Figure 16. Cylindrical bubble trap with two levitated sonoluminescing bubbles. The bubbles blink alternately, each with a frequency of the sound field of 25.8 kHz.

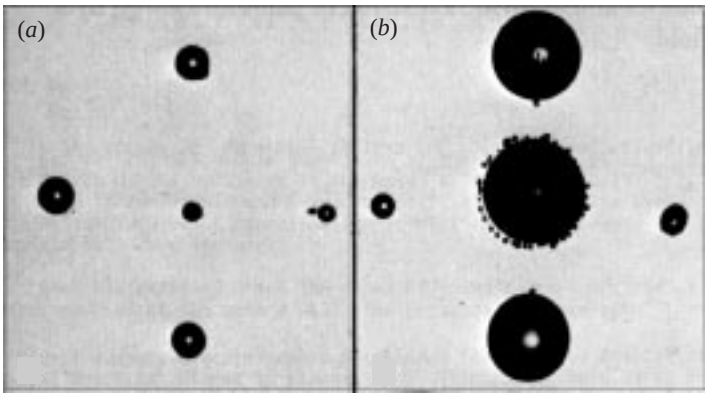

Figure 17. Five-bubble systems in silicone oil formed by single multifocus Q-switched ruby laser pulses: (*a*) shows that significant bubble interaction takes place (note the appearance of satellite microbubbles).

optical elements) almost any initial configuration of bubbles is producible. An example is given in figure 17. Even bubble generation at different times in different places is feasible, giving some control over the phase relationship of the bubbles (Tomita & Shima 1990). Though still in their infancy, investigations such as these will be required to fully understand the complicated processes taking place in multibubble systems, and, in particular, in multibubble sonoluminescence (MBSL) with its characteristic differences to SBSL (Matula *et al*. 1995).

5. Multibubble dynamics

Multibubble systems are encountered naturally in acoustic cavitation experiments and in many practical situations, e.g. in hydrodynamic cavitation near ship propellers or in sonochemistry. As truly three-dimensional multiparticle systems, they pose a great challenge to the experimentalist when setting out to capture the full spatio-temporal dynamics of the bubble field. Usually, rather coarse-grained measurements have been performed, e.g. the recording and analysis of the acoustic signal (cavitation noise) or of the scattering or transmission of light by the bubble cloud (figure 18). The beam of a He:Ne laser is expanded and directed along the axis of a piezoceramic cylinder where it penetrates the cavitation zone. The laser light is scattered, the

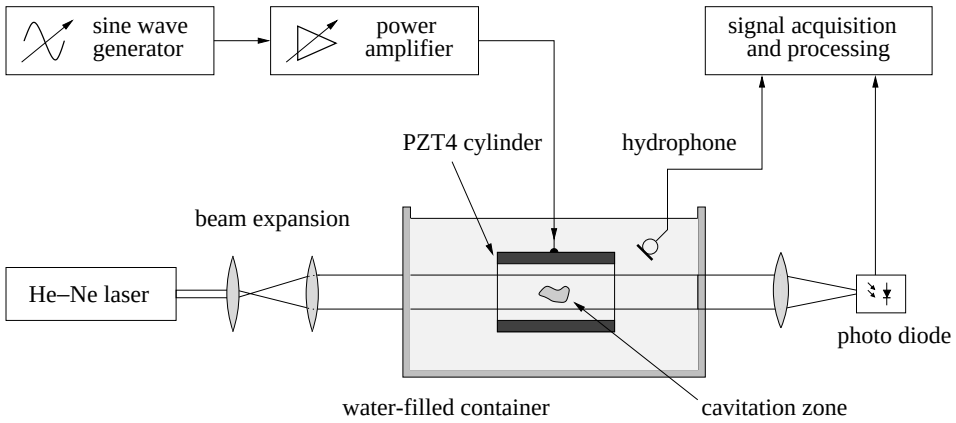

Figure 18. Arrangement for a light transmission experiment with cavitation noise processing.

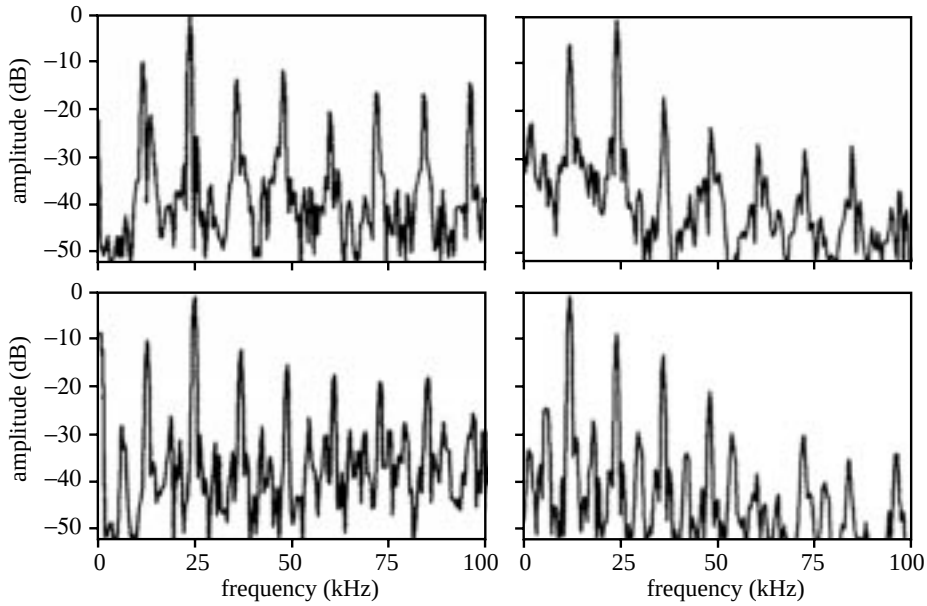

Figure 19. Comparison of the acoustic spectra of cavitation noise (left) and the power spectra of the light transmission signal (right) obtained with the arrangement of figure 18 for two different driving pressures at frequency $f_0 = 23.1$ kHz: (top row) subharmonic response giving multiples of $\frac{1}{2}f_0$; (bottom row) response giving multiples of $\frac{1}{4}f_0$.

amount of scattering being dependent on the bubble sizes. The transmitted light, which is collected by a lens and focused onto a photodiode, decreases in proportion to the total scattering cross-section.

In figure 19 the acoustic spectrum derived from the hydrophone signal is compared to the modulation spectrum of the transmitted light signal for two measurements at a driving frequency of 23.1 kHz. It becomes clear that the qualitative features of both signals, e.g. the appearance of harmonics or subharmonics in the spectrum, are the same for the two types of signals.

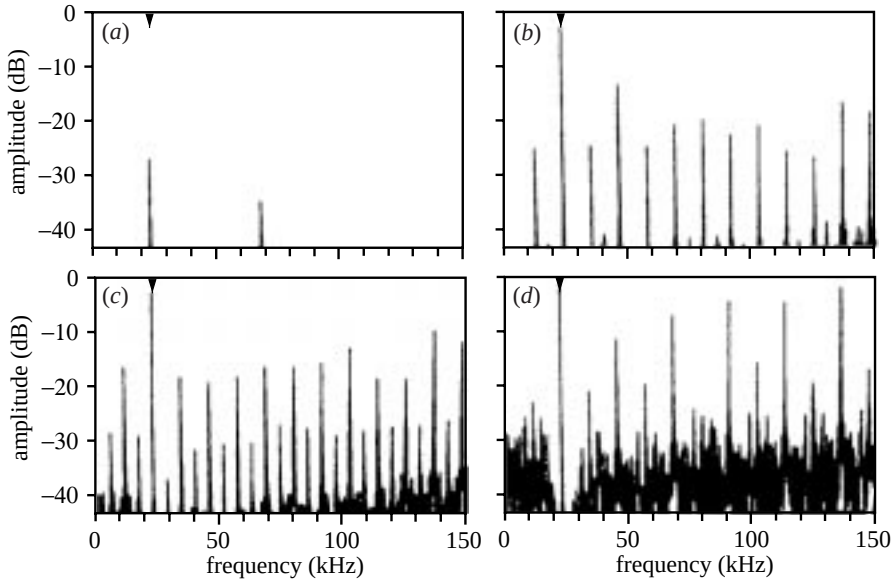

Figure 20. Power spectra of cavitation noise taken at a driving frequency of $f_0 = 23$ kHz, marked in the figures by a small upside down triangle. The driving pressure was increased from one graph to the next, giving first a periodic anharmonic signal (a), then subharmonic motion with lines at multiples of $\frac{1}{2}f_0$ (period-2 motion) (b), then period-4 motion with lines at multiples of $\frac{1}{4}f_0$ (c), and finally a broadband spectrum indicative of chaotic behaviour (d).

(*a*) *Collective dynamics*

Let us further concentrate on the hydrophone signal. Obviously, it is generated by the superposition of a multitude of acoustic emissions from bubbles within the container. It has, therefore, to be viewed as an integral observable of the multibubble field. Thus, the discovery that the acoustic signal shows clear-cut dynamical features (e.g. period-doubling bifurcations) that can be attributed to the radial dynamics of a single bubble came as a great surprise! This finding gives strong support to the hypothesis that the individual bubbles oscillate in the sound field in a largely synchronous fashion. The synchrony conjecture is also corroborated by the reported correlation between the acoustic and light transmission signals, since all bubbles contribute to the light scattering according to their size.

Figure 20 gives a sequence of spectra from a number of sections of a measured hydrophone signal. It was recorded with a cavitation cylinder driven by a carefully adjusted amplitude-swept signal. The figure demonstrates the occurrence of periodic oscillation, then subharmonic (period-2) oscillation, followed by period-4 oscillation. This sequence is indicative of a period-doubling sequence commonly encountered in nonlinear dynamical systems when one of the system parameters is varied, and in particular in the radial dynamics of cavitation bubbles driven by a sound field (Parlitz *et al*. 1990).

It is well known that such a bifurcation sequence constitutes one road to chaotic behaviour. In fact, the power spectrum of the acoustic signal beyond the period-doubling regime has a broad-band character which may well originate in deterministic–chaotic dynamics (figure 20*d*). Fourier spectra are not very helpful here in deter-

mining true noise from chaos. Therefore, methods of nonlinear time-series analysis (e.g. attractor reconstruction by embedding, calculation of fractal dimensions and Lyapunov spectra (Lauterborn & Parlitz 1988)), have been employed to assess the deterministic origin of the signal. For example, its phase-space reconstruction yields an irregular-looking trajectory with all the features of a chaotic attractor.

These results demonstrate that much can be learned about acoustic cavitation from the measurement of just a single averaged quantity. This is a very fortunate property of bubble ensembles which may be attributed to their tendency to oscillate coherently and thus to exhibit low-dimensional dynamics, at least on a coarse-grained scale.

To really understand the occurrence of low-dimensional dynamics and many other aspects of multibubble systems, it is desirable to tackle the difficult experimental problem of capturing the whole spatio-temporal dynamics within a certain volume of the liquid. High-speed photography or cinematography are a first step in accomplishing this task. Their drawbacks are a limited depth of view and the possible obstruction of bubbles by other bubbles positioned in the foreground. Remedy is provided, at least partly, by holographic methods, in their ultimate form by high-speed holographic cinematography. By exploiting the three-dimensional character of image reconstruction of high-speed holograms, it is possible to obtain views of the bubble distribution at different depths of field and at different viewing angles. The bubble distribution and bubble dynamics are all stored in a holographic series and can be retrieved, up to the limits imposed by optical and temporal resolution, by extensive off-line analysis of the holograms.

The potential of high-speed holographic methods is demonstrated in figure 21, which depicts reconstructed images taken from several high-speed holographic series (Lauterborn & Koch 1987). They were taken of a cavitation field in synchrony with the applied driving frequency, at different stages of a period-doubling sequence. The holographic series reveals that the bubble field oscillates as a whole in the periodic mode indicated by the acoustic spectrum. The spectra corresponding to the image rows of figure 21 are reproduced in figure 22. As far as the limited optical resolution allows, one can state that all bubbles seem to oscillate in synchrony, repeating their pattern after one driving period (first row), after two driving periods (second row), after four driving periods (third and forth row) and after eight driving periods (fifth and sixth row), in accordance with the associated acoustic spectrum. High-speed holography has thus given us direct evidence for the coherence of bubble oscillations, which we have postulated previously from the results of cavitation noise analysis.

(*b*) *Multibubble sonoluminescence (MBSL)*

We have discussed before that single bubbles, if they collapse sufficiently undisturbed, may emit light. Light emission, later termed sonoluminescence, was first discovered for multibubble systems in 1933. It was observed that photographic plates immersed into a water container are blackened by ultrasonic irradiation (Marinesco & Trillat 1933). It soon became clear that the effect was due to the light emission that accompanied acoustic cavitation (Frenzel & Schultes 1934).

Figure 23 shows a photograph of MBSL taken with modern equipment—a highly sensitive image-intensified CCD camera. The faint glow of a bubble cloud in a cavitation cylinder was observed with no further illumination at a long exposure time

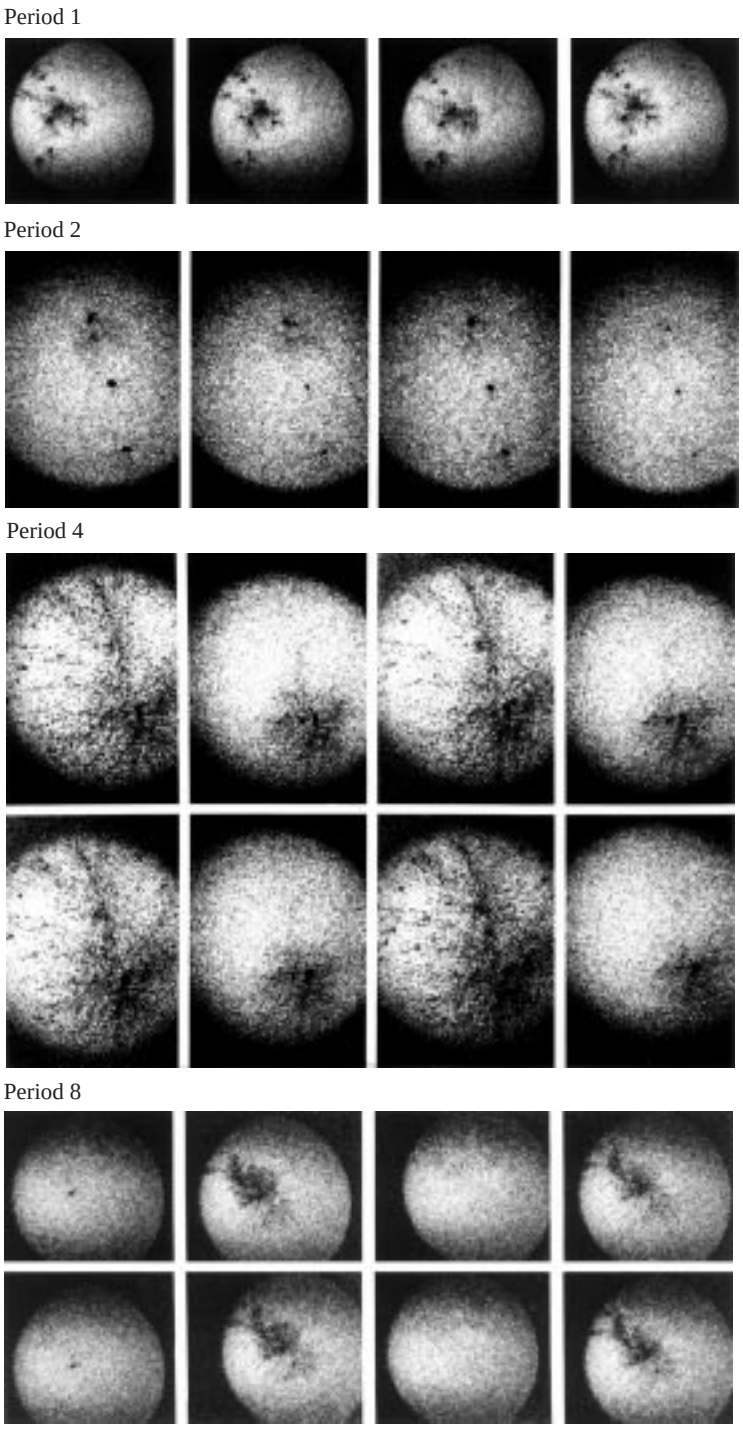

Figure 21. High-speed holographic images of a bubble field driven at 23.1 kHz. One hologram was taken per period of the driving field. The bubble field oscillates periodically as a whole with the indicated period.

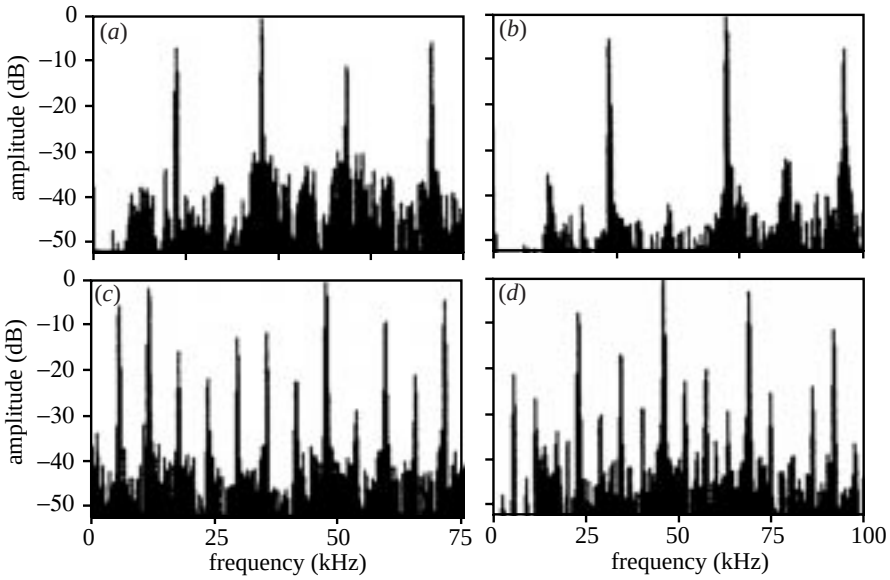

Figure 22. Acoustic spectra recorded simultaneously with the holographic series of figure 21. They belong to different stages in a period-doubling cascade: (*a*) period-1; (*b*) period-2; (*c*) period-4; (*d*) period-8.

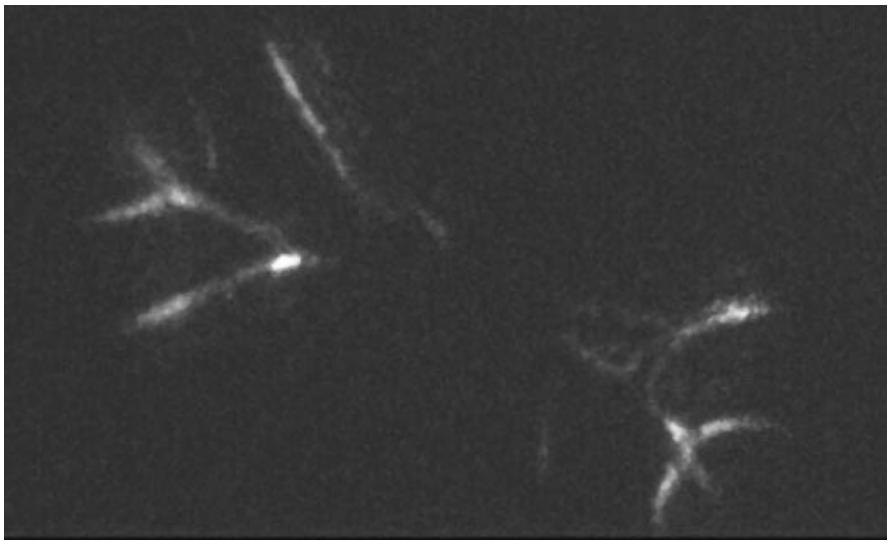

Figure 23. Long-time exposure revealing the faint light emission of bubbles in a cavitation cylinder. The image-intensified CCD picture shows that the spatial distribution of sonoluminescence is correlated with the bubble structure (streamers) in the sound field.

to collect sufficient light. The SL emission reflects quite well the structure of bubble distribution, obviously so stable on the average as to be visible in the picture.

After the discovery of sonoluminescence, subsequent studies over the following decades, at a moderate pace in this not too-overpopulated branch of physics, revealed many properties of the phenomenon, in particular the fact that the light emission is

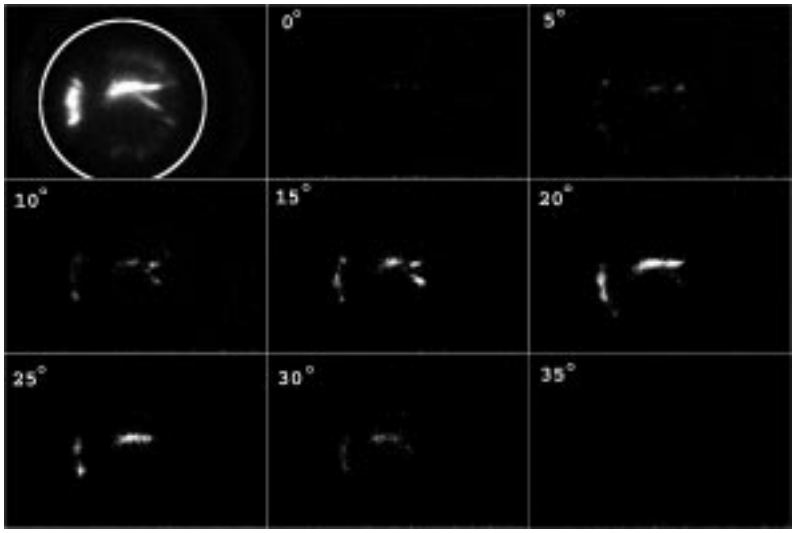

Figure 24. The light emission from a bubble ensemble takes place in a narrowly defined phase window with respect to the driving signal. The images show ICCD images gated a large number of times at the indicated phase (the zero phase being chosen arbitrarily). The top-left picture gives the integrated view of the luminescing bubble field with an outline of the cavitation cylinder.

closely related to violent bubble collapse (Meyer & Kuttruff 1959). The result of an experiment to demonstrate the phase relationship between light emission and driving pressure (thus, bubble collapse), conducted with a gated ICCD camera, is presented in figure 24. It is seen that in a multibubble field the single luminescence events are not distributed evenly over the acoustic cycle, and all take place within a narrow phase window of the drive period.

For MBSL the influence of parameters such as composition and temperature of the liquid, its gas content, acoustic pressure, dissolved substances, etc., has been thoroughly studied, as well as the spectral features of the light. For a detailed account of the development of the subject and of experimental facts, the reader is referred to the literature, in particular to the review by Walton & Reynolds (1984). When comparing the experimental findings of SBSL and MBSL, respectively, certain differences between the two phenomena become evident. For example, spectroscopic measurements have revealed that MBSL can be assigned a temperature of about 5000–6000 K (Günther *et al*. 1959; Flint & Suslick 1991), obviously smaller than the value found for SBSL. Furthermore, unlike SBSL spectra, the MBSL light features spectral lines and band emission, e.g. by OH^- radicals or from dissolved salt (Matula *et al*. 1995). On the other hand, both phenomena share a number of properties, e.g. the strong influence of noble gases on light intensity.

Thus the question arises: how are SBSL and MBSL related? This important subject is still under debate. It is closely connected with the question as to the role of spherical symmetry in bubble luminescence. Crum (1994) has put forward an interesting conjecture about the difference between MBSL and SBSL. He suggests that SBSL is intrinsically different from MBSL in that SBSL is fuelled by a shock wave in the gas of a symmetrically collapsing bubble, while MBSL is due to incandescence of the host liquid by the liquid jet generated during asymmetric collapse. On the other

hand, there are theories, like that of Prosperetti (1997), which also invoke asymmetric bubble collapse in the case of SBSL. The results on single-bubble dynamics collected in this paper give strong evidence for the necessity of a certain degree of spherical symmetry of the collapsing bubble as a prerequisite for light generation. Furthermore, in all data collected so far the light emitting region is well defined in a single spot, located at the centre of the bubble before collapse.

While laser-generated bubbles are different from stably levitated bubbles in some respects, we are confident that a further exploration of cavitation bubble luminescence in optical cavitation can also shed light on the sonoluminescence phenomenon. After all, in both cases it is a collapsing bubble that produces the light, and the findings presented are consistent with the presence of converging shock waves within the bubble in both cases. With single laser-generated bubbles near a boundary or with few-bubble systems it will be possible to simulate the environment of MBSL locally and to study the light emission there with high temporal and spatial resolution. Furthermore, with laser-generated bubbles we are not restricted to the parameter space accessible to small bubbles in diffusive equilibrium and thus may achieve considerably more light by a more violent collapse. This facilitates spectroscopic studies, for example.

6. Conclusions

In this paper we have adopted a wholly experimental approach to bubble dynamics. A number of experimental results on single- and multibubble systems, mainly obtained by high-speed photographic or holographic methods and by the analysis of the bubbles' acoustic emission, have been reviewed to elucidate the details of spherical and aspherical bubble collapse under different conditions. In particular, the radial dynamics and shock-wave emission of single stably levitated sonoluminescing bubbles have been demonstrated by direct optical observation. The dynamics and light emission properties of symmetrically and asymmetrically collapsing laser-generated bubbles were presented in detail. The results clearly show that single-cavitation bubble luminescence is suppressed with sufficiently asymmetric collapse.

Optic cavitation is advocated as an alternative approach to the study of light emission by bubbles. Though the physical parameters and dynamical boundary conditions are different for stably levitated bubbles and transient laser-generated bubbles, we suppose the physical mechanism of light emission, in particular the existence of strong inhomogeneities in the bubble interior, to be similar in both phenomena.

For establishing a firmer link between SBSL and SCBL based on quantitative data, further experiments as well as theoretical and numerical modelling of asymmetric bubble collapse are required and are now being approached. First, the dependence of SCBL on experimental parameters such as temperature, gas concentration or composition of the liquid have to be investigated systematically. In particular, the influence of noble-gas content of the liquid on luminescence intensity of laser-generated bubbles is an important issue. Also, experiments with shorter laser pulses which yield smaller bubbles are currently being performed, bringing laser-produced bubbles down to approximately the size of SBSL bubbles.

To allow for a direct comparison between experimentally observed light-emission properties and those predicted by current models, it is necessary to numerically simulate shock-wave formation in asymmetrically collapsing cavities. This quite formid-

able free-boundary problem may require new modelling approaches such as molecular dynamics, whose prospects for bubble simulation are now being investigated.

Thus, a wealth of experiments and challenges for modelling lie ahead in optical cavitation and bubble luminescence. With high-speed and ultrafast optical instruments as well as powerful computers, we hopefully will gather new insights into the fascinating but complex world of bubbles.

The authors thank all the members of the cavitation and sonoluminescence group of the Third Physics Institute for lively and fruitful discussions, and, in particular, Cordt Schenke for his participation in experiments on laser-induced breakdown.

References

Barber, B. P., Wu, C. C., Löfstedt, R., Roberts, P. H. & Putterman, S. J. 1994 Sensitivity of sonoluminescence to experimental parameters. *Phys. Rev. Lett.* **72**, 1380–1383.

Barber, B. P., Hiller, R. A., Löfstedt, R., Putterman, S. & Weninger, K. R. 1997 Defining the unknowns of sonoluminescence. *Phys. Rep.* **281**, 65–143.

Brennen, C. E. 1995 *Cavitation and bubble dynamics*. Oxford University Press.

Buzukov, A. A. & Teslenko, V. S. 1971 Sonoluminescence following focusing of laser radiation into a liquid. *Soviet Phys. JETP Lett.* **14**, 189–191.

Crum, L. A. 1994 Sonoluminescence, sonochemistry, and sonophysics. *J. Acoust. Soc. Am.* **95**, 559–562.

Flint, E. B. & Suslick, K. S. 1991 The temperature of cavitation. *Science* **253**, 1397–1399.

Frenzel, H. & Schultes, H. 1934 Luminescenz im ultraschallbeschickten Wasser. *Z. Phys. Chem.* **27b**, 421–424.

Gaitan, F. D., Crum, L. A., Church, C. C. & Roy, R. A. 1992 Sonoluminescence and bubble dynamics for a single, stable, cavitation bubble. *J. Acoust. Soc. Am.* **91**, 3166–3183.

Gompf, B., Günther, R., Nick, G., Pecha, R. & Eisenmenger, W. 1997 Resolving sonoluminescence pulse width with time-correlated single photon counting. *Phys. Rev. Lett.* **79**, 1405–1408.

Günther, P., Heim, E. & Borgstedt, H. U. 1959 Über die kontinuierlichen Sonolumineszenzspektren wäßriger Lösungen. *Z. Elektrochem.* **63**, 43–47.

Heim, E 1961 Über das Zustandekommen der Sonolumineszenz. In *Proc. 3rd Int. Cong. on Acoustics, Stuttgart, 1959* (ed. L. Cremer), pp. 343–346. Amsterdam: Elsevier.

Hiller, R., Putterman, S. J. & Barber, B. P. 1992 Spectrum of synchronous picosecond sonoluminescence. *Phys. Rev. Lett.* **69**, 1182–1184.

Holt, R. G. & Gaitan, D. F. 1996 Observation of stability boundaries in the parameter space of single bubble sonoluminescence. *Phys. Rev. Lett.* **77**, 3791–3794.

Kedrinskii, V. K. 1997 The role of cavitation effects in the mechanisms of destruction and explosive processes. *Shock Waves* **7**, 63–76.

Lauterborn, W. (ed.) 1980 *Cavitation and inhomogeneities in underwater acoustics*. Berlin: Springer.

Lauterborn, W. & Koch, A. 1987 Holographic observation of period-doubled and chaotic bubble oscillations in acoustic cavitation. *Phys. Rev.* A **35**, 1974–1976.

Lauterborn, W. & Parlitz, U. 1988 Methods of chaos physics and their application to acoustics. *J. Acoust. Soc. Am.* **84**, 1975–1993.

Leighton, T. G. 1994 *The acoustic bubble*. London: Academic.

Marinesco, M. & Trillat, J. J. 1933 Action des ultrasons sur les plaques photographiques. *Compt. Rend.* **196**, 858–860.

Matula, T. J., Roy, R. A., Mourad, P. D., McNamara III, W. B. & Suslick, K. S. 1995 Comparison of multibubble and single-bubble sonoluminescence spectra. *Phys. Rev. Lett.* **75**, 2602–2605.

Mettin, R., Akhatov, I., Parlitz, U., Ohl, C. D. & Lauterborn, W. 1997 Bjerknes forces between small cavitation bubbles in a strong acoustic field. *Phys. Rev.* E **55**, 2924–2931.

Meyer, E. & Kuttruff, H. 1959 Zur Phasenbeziehung zwischen Sonolumineszenz und Kavitationsvorgang bei periodischer Anregung. *Z. Ang. Phys.* **11**, 325–333.

Moran, M. J. & Sweider, D. 1998 Measurements of sonoluminescence temporal pulse shape. *Phys. Rev. Lett.* **80**, 4987–4990.

Moss, W. C., Clarke, D. B. & Young, D. A. 1997 Calculated pulse widths and spectra of a single sonoluminescing bubble. *Science* **276**, 1398–1401.

Ohl, C. D., Philipp, A. & Lauterborn, W. 1995 Cavitation bubble collapse studied at 20 million frames per second. *Ann. Phys.* **4**, 26–34.

Ohl, C.-D., Lindau, O. & Lauterborn, W. 1998 Luminescence from spherically and aspherically collapsing laser induced bubbles. *Phys. Rev. Lett.* **80**, 393–396.

Parlitz, U., Englisch, V., Scheffczyk, C. & Lauterborn, W. 1990 Bifurcation structure of bubble oscillators. *J. Acoust. Soc. Am.* **88**, 1061–1077.

Philipp, A. & Lauterborn, W. 1998 Cavitation erosion by single laser-produced bubbles. *J. Fluid Mech.* **361**, 75–116.

Prosperetti, A. 1997 A new mechanism for sonoluminescence. *J. Acoust. Soc. Am.* **101**, 2003–2007.

Rayleigh, Lord 1917 On the pressure developed in a liquid during the collapse of a spherical cavity. *Phil. Mag.* **34**, 94–98.

Rein, M. 1993 Phenomena of liquid drop impact on solid and liquid surfaces. *Fluid Dynamics Res.* **12**, 61–93.

Tian, Y., Ketterling, J. A. & Apfel, R. E 1996 Direct observation of microbubble oscillations. *J. Acoust. Soc. Am.* **100**, 3976–3978.

Tomita, Y. & Shima, A. 1990 High-speed photographic observations of laser-induced cavitation bubbles in water. *Acustica* **71**, 161–171.

Vogel, A., Lauterborn, W. & Timm, R. 1989 Optical and acoustic investigations of the dynamics of laser-produced cavitation bubbles near a solid boundary. *J. Fluid Mech.* **206**, 299–338.

Walton, A. J. & Reynolds, G. T. 1984 Sonoluminescence. *Adv. Phys.* **33**, 595–660.

Weninger, K. R., Barber, B. P. & Putterman, S. J. 1997 Pulsed Mie scattering measurements of the collapse of a sonoluminescing bubble. *Phys. Rev. Lett.* **78**, 1799–1802.

Wu, C. C. & Roberts, P. H. 1994 A model of sonoluminescence. *Proc. R. Soc. Lond.* A **445**, 323–349.